



# The high sensitivity of SMOS L-Band vegetation optical depth to biomass

Nemesio J. Rodríguez-Fernández<sup>1</sup>, Arnaud Mialon<sup>1</sup>, Stephane Mermoz<sup>1</sup>, Alexandre Bouvet<sup>1</sup>, Philippe Richaume<sup>1</sup>, Ahmad Al Bitar<sup>1</sup>, Amen Al-Yaari<sup>2</sup>, Martin Brandt<sup>3</sup>, Thomas Kaminski<sup>4</sup>, Thuy Le Toan<sup>1</sup>, Yann H. Kerr<sup>1</sup>, and Jean-Pierre Wigneron<sup>2</sup>

<sup>1</sup>Centre d'Etudes Spatiales de la Biosphère (CESBIO), Centre National d'Etudes Spatiales (CNES), Centre National de la Recherche Scientifique (CNRS), Institut de Recherche pour le Développement (IRD), Université Paul Sabatier, Université de Toulouse, 18 av. Edouard Belin, bpi 2801, 31401 Toulouse, France

<sup>2</sup>Interactions Sol Plante Atmosphère (ISPA), Unité Mixte de Recherche 1391, Institut National de la Recherche Agronomique (INRA), CS 20032, 33882 Villenave d'Ornon cedex, France

<sup>3</sup>Department of Geosciences and Natural Resources Management, University of Copenhagen, 1350 Copenhagen, Denmark

<sup>4</sup>The inversion Lab, Hamburg, Germany

*Correspondence to:* N.J. Rodríguez-Fernández ([nemesio.rodriguez-fernandez@univ-tlse3.fr](mailto:nemesio.rodriguez-fernandez@univ-tlse3.fr))

**Abstract.** The vegetation optical depth (VOD) measured at microwave frequencies is related to the vegetation water content and provides information complementary to visible/infra-red vegetation indices. This study is devoted to the characterisation of a new VOD data set obtained from SMOS (Soil Moisture and Ocean Salinity) satellite observations at L-band (1.4 GHz). Three different SMOS L-band VOD (L-VOD) data sets (SMOS Level 2, Level 3 and SMOS-IC) were compared with data sets on tree height, visible/infra-red indexes (NDVI, EVI), cumulated precipitation, and above ground biomass (AGB) for the African continent. For all relationships, SMOS-IC showed the lowest dispersion and highest correlation. Overall, we found a strong ( $R > 0.85$ ) correlation with no clear sign of saturation between L-VOD and four AGB data sets. The relationship linking L-VOD to tree height ( $R = 0.87$ ) and Baccini's AGB ( $R = 0.94$ ) was strong and linear. The relationships between L-VOD and three other AGB data sets were linear per land cover class, but with a changing slope depending on the land cover type. For low vegetation classes, the annual mean of L-VOD spans a range from 0 to 0.7 and it is linearly correlation with the amount of the average annual precipitations. SMOS L-VOD showed a higher sensitivity to AGB as compared to NDVI and K/X/C-VOD (VOD measured, respectively, at 19, 10.7, and 6.9 GHz). The results showed that although the spatial resolution of L-VOD is coarse ( $\sim 40$  km), the high temporal frequency and sensitivity to AGB makes SMOS L-VOD a very promising index for large scale monitoring of the vegetation status, in particular biomass.

## 1 Introduction

Large scale monitoring of vegetation properties is crucial to understand water, carbon and energy cycles. The Normalized Difference Vegetation Index (NDVI, Tucker, 1979) computed from space-borne observations at visible and infra-red wavelengths has been widely used since the 1980s to study vegetation changes and its implications on animal ecology (Pettorelli et al., 2005, 2011), global fire emissions (Van der Werf et al., 2010), deforestation and urban development (Esau et al., 2016), global



20 patterns of land-atmosphere carbon fluxes (Jung et al., 2011) and the vegetation response to climate (Herrmann et al., 2005) and extreme events such as droughts (Vicente-Serrano et al., 2013). NDVI is sensitive to the abundance of chlorophyll and therefore to the photosynthetically active biomass (which includes herbaceous vegetation and the leaves of trees), but insensitive to wood mass. NDVI is thus not considered as an accurate proxy of total above ground biomass (AGB), except in areas of low vegetation density (Todd et al., 1998). Contrastingly, being sensitive to both green and non-green vegetation components, passive microwave observations can provide important complementary information on the state and time changes of the vegetation features, in particular regarding the AGB dynamics (Liu et al., 2015).

The thermal emission arising from the Earth surface at microwave frequencies depends on the soil characteristics such as soil temperature, soil roughness and soil moisture content, which controls the soil emissivity (Ulaby, 1976). In the presence of vegetation, part of the soil emission is absorbed and scattered. This extinction effect is parameterized by the vegetation optical depth (VOD) that can be estimated using radiative transfer theory (Mo et al., 1982; Ulaby and Wilson, 1985; Ferrazzoli and Guerriero, 1996; Wigneron et al., 2007; Liu et al., 2011). VOD was shown to be linked to the vegetation water content (VWC, kg/m<sup>2</sup>) (Kirdiashev et al., 1979; Mo et al., 1982; Jackson and Schmugge, 1991) and to other vegetation properties such as the Leaf Area Index (Jackson and Schmugge, 1991; Van de Griend and Wigneron, 2004; Wigneron et al., 2007). VOD is also a function of the vegetation structure which determines its dependence on the incidence angle and on the polarization of the radiation (Ulaby and Wilson, 1985; Wigneron et al., 1995, 2004; Hornbuckle et al., 2003; Schwank et al., 2005).

Passive microwave radiometry is therefore a promising tool to monitor the vegetation at global scale. VOD samples a thick layer of the vegetation canopy including woody vegetation, which uses root zone soil moisture (Andela et al., 2013). VOD was used to study deforestation in South America (Van Marle et al., 2016) and Africa (Brandt et al., 2017). Using VOD, it has been possible to reveal teleconnections linking the state of the vegetation in Australia and El Niño Southern Oscillation (Liu et al., 2007). In addition, Liu et al. (2015) showed the high potential of microwave VOD to monitor the AGB dynamics at large scale. Using both VOD and NDVI contributes to provide a more robust assessment of the vegetation characteristics (Liu et al., 2011).

The above mentioned studies used VOD derived from different radiometers operating at different frequencies (Liu et al., 2011): SSM/I at 19 GHz (K-band), TRMM-TMI at 10.7 GHz (X-band), and the Advanced Microwave Scanning Radiometer - Earth Observing System (AMSR-E) at 10.7 GHz and 6.9 GHz (C-band). It is worth noting that VOD is intrinsically dependent on the frequency of the electromagnetic radiation and VODs retrieved at different frequencies provide complementary information. Therefore, in the following, a specific VOD data set will be noted as *B*-VOD, where *B* stands for the microwave band (X-VOD, C-VOD,...). The lower the frequency, the lower the VOD for a given level of VWC (Wigneron et al., 1995, 2004; Ferrazzoli and Guerriero, 1996). Consequently, L-band (1.4 GHz, 21 cm) observations, which are less attenuated through the vegetation canopy, are capable of sampling the vegetation layer up to higher biomass values compared to higher frequency observations.

Currently, two missions are performing systematic L-band passive microwave observations: The Soil Moisture and Ocean Salinity (SMOS) satellite (Kerr et al., 2010), launched by ESA in November 2009, and the Soil Moisture Active Passive (SMAP) satellite (Entekhabi et al., 2010), launched by NASA in January 2015. The full-polarization and multi-angular capabilities of SMOS allow to retrieve simultaneously the soil moisture content and L-VOD. Lawrence et al. (2014) and Grant et al.



35 (2016) compared SMOS L-VOD to X-VOD and C-VOD measured by AMSR-E and to visible/infra-red vegetation indices. In  
crop zones, as the MODIS vegetation indices, L-VOD increases during the growing season and decreases during senescence  
(Lawrence et al., 2014). At global scale, L-VOD is less correlated to optical/visible vegetation indices than X/C-VOD, suggest-  
ing that L-VOD can add more complementary information with respect to optical/infrared indices than X/C-VOD (Grant et al.,  
2016). For instance, Rahmoune et al. (2014) found a significant correlation between L-VOD and tree height estimates. Vittucci  
5 et al. (2015) also discussed this relationship and compared it to the one estimated with X/C-VOD, which shows higher values  
for low tree-height than SMOS L-VOD, as expected. Vittucci et al. (2015) also showed a close to linear relationship between  
L-VOD and AGB at 20 selected points over Peru, Columbia, and Panama.

In summary, L-VOD derived from the new SMOS L-Band observations is a promising tool for monitoring global vegetation  
characteristics. There is, however, a lack of in-depth studies on how L-VOD relates to established vegetation characteristics. The  
10 goal of the current study is to get further insight into the sensitivity of L-VOD to vegetation properties and precipitations, which  
can drive the vegetation dynamics for some biomes. Taking into account the novelty of these observations, three distinct SMOS  
L-VOD data sets were evaluated against several data sets independent of L-VOD: (i) optical/infra-red indices (representing the  
greenness of vegetation, also often used as proxy for primary productivity), (ii) AGB benchmark maps, (iii) LIDAR derived tree  
height and (iv) precipitation data set. The area selected for this study is Africa, as it is a continent with several climate regions  
15 and biomes and with a large variability in the vegetation biomass from sparse shrubs to savannah and very dense rainforests.  
In addition, Bouvet et al. (2018) have recently discussed the first biomass map of African savannahs computed from L-band  
active microwave (synthetic aperture radar) observations.

The document is organized as follows. Section 2 presents the different SMOS L-VOD data sets as well as the data sets  
used for the evaluation (tree height, cumulated precipitations, NDVI, EVI and four AGB data sets). Section 3 deals with the  
20 evaluation methods. Section 4 presents the results, which are discussed in Section 5, in particular the potential of L-VOD to  
estimate AGB at large scale. Finally, Section 6 summarizes the results and presents the conclusions of this study.

## 2 Data

### 2.1 SMOS data

The SMOS (Kerr et al., 2001, 2010) mission is an ESA-led mission with contributions from CNES (Centre National d'Etudes  
25 Spatiales, France) and CDTI (Centro Para el Desarrollo Tecnológico Industrial, Spain). The SMOS radiometer measures the  
thermal emission from the Earth in the protected frequency range around 1.4 GHz in full-polarization and for incidence angles  
from 0° to ~ 60°. The footprint (full width at half maximum of the synthesized beam) is ~ 43 km on average (Kerr et al.,  
2010). The equator overpass time is 6:00 AM/PM for ascending/descending orbits. Only ascending orbits are used in this study  
as the overall quality of the data is higher than the descending data. Taking into account the novelty of L-VOD estimates,  
30 three different L-VOD data sets were evaluated in this study: the ESA Level 2 (L2) product, the CATDS multi-orbit Level 3  
(L3) product and the new INRA-CESBIO (IC) data set. The differences between these data sets are discussed in the following  
(Table S1 gives a summary of the main characteristics of those three products).



### 2.1.1 SMOS Level 2 soil moisture and L-VOD

The SMOS soil moisture and L-VOD L2 retrieval algorithm was described by Kerr et al. (2012). The algorithm uses the L-MEB (L-band Microwave Emission of the Biosphere) radiative transfer model (Wigneron et al., 2007), which is based on the  $\tau - \omega$  (optical depth - single scattering albedo) parameterization to take into account the effect of vegetation. The difference between forward model estimates of the brightness temperatures at antenna reference frame and actual satellite measurements is minimized by varying the values of the soil moisture (SM) content and the L-VOD. The contributions from the soil and vegetation layers can be distinguished thanks to the multi-angular and dual-polarization measurements. The soil temperature profile is estimated from European Centre for Medium Range Weather Forecasts (ECMWF) Integrated Forecast System (IFS) data. The forward model contributions are computed at  $\sim 4$  km resolution pixels and aggregated to the sensor resolution using the mean synthetic antenna pattern. For footprints with mixed land cover, the L2 algorithm distinguishes the minor and the major land cover (low vegetation or forest). The SMOS retrieval is performed only over the dominant land cover class within the footprint while the emission of the minor land cover is estimated from ECMWF SM and MODIS Leaf Area Index (LAI) data (Kerr et al., 2012). The version of the data used in the current study is 620. This data version uses auxiliary files including information on L-VOD computed from previous retrievals, surface roughness and Radio Frequency Interference (RFI) that are used to constrain the new retrievals. The SMOS L2 data are provided by ESA in an Icosahedral Equal Area (ISEA) 4H9 grid (Sahr et al., 2003) in swath mode with a sampling resolution of 15 km.

### 2.1.2 SMOS Level 3 soil moisture and L-VOD

The SMOS L3 soil moisture and L-VOD data set is provided by the CATDS (Centre Aval de Traitement de Données SMOS) from CNES (Centre National D'Etudes Spatiales) and IFREMER (Institut Français de Recherche pour l'Exploitation de la Mer) in an Equal-Area Scalable Earth (EASE) grid version 2 (Brodzik et al., 2012.) with a sampling resolution of 25 km. The data version used in this study is Version 300. The data set and the retrieval algorithm are described in Al Bitar et al. (2017). The L3 algorithm is based on the same physics and modelling as the ESA L2 single-orbit algorithm (Section 2.1.1). Instead of using information on prior retrievals to constrain the SM and L-VOD inversion, the Level 3 algorithm uses a multi-orbit approach with data from three different revisits over a seven day window. In contrast to soil moisture, L-VOD is not expected to change strongly over a short period of time. Therefore a Gaussian correlation function is used during the retrieval to penalize large L-VOD variations in the cost function. The standard deviation of the Gaussian correlation function is 21 days for forests and 7 days for low vegetation (Al Bitar et al., 2017).

### 2.1.3 SMOS INRA-CESBIO (IC) soil moisture and L-VOD

The SMOS INRA-CESBIO (SMOS-IC) algorithm was designed by INRA (Institut National de la Recherche Agronomique) and is produced by CESBIO (Centre d'Etudes Spatiales de la BIOSphère). A detailed description is given in Fernandez-Moran et al. (2017). One of the main goals of the SMOS-IC product is to be as independent as possible from auxiliary data, which are often also used for evaluation. SMOS-IC is based on the same L-MEB (Wigneron et al., 2007) model used by the ESA L2



algorithm (Section 2.1.1) to perform global retrievals of SM and L-VOD but it uses some simplifications. In contrast to the L2 and L3 algorithms, the IC algorithm considers the footprints to be homogeneous to avoid uncertainties and errors linked to possible inconsistencies in the auxiliary data sets which are used to characterize the footprint heterogeneity. As for the L2 and L3 algorithms, the soil temperature profile is estimated from ECMWF Integrated Forecast System (IFS) data. However, SMOS-IC differs from the SMOS L2 and L3 products in the initialization of the cost function minimization and in the modelling of heterogeneous pixels: no LAI nor ECMWF SM data are used. Finally, the effective vegetation scattering albedo and soil roughness parameters were optimized as discussed by Fernandez-Moran et al. (2017) and are different to those used by the Level 2 and Level 3 algorithms. The data used in this study is version 103 and it is provided in the 25 km EASEv2 grid.

## 2.2 Evaluation data sets

- 10 This study performs an evaluation of the SMOS L-VOD data sets by a comparison with other vegetation-related evaluation data sets which are described in the following.

### 2.2.1 Precipitations

- 15 The Worldclim data set provides spatially interpolated monthly climate data for global land areas at a very high spatial resolution (approximately 1 km). It includes monthly temperature (minimum, maximum and average), precipitation, solar radiation, vapour pressure and wind speed, aggregated across a target temporal range of 1970-2000, using data from between 9000 and 60 000 weather stations. As precipitations drive the vegetation dynamics for some biomes, mean annual precipitation were used to evaluate the relationship with L-VOD.

### 2.2.2 MODIS vegetation indices

- 20 MODIS NDVI and Enhanced Vegetation Index (EVI) from the product MYD13C1 (Huete et al., 2002) collection 6 were compared to the SMOS L-VOD data sets to test L-VOD's performance against green photosynthetically active vegetation. Both NDVI and EVI are directly linked to the sential climate variables FAPAR and LAI and they are widely used as proxy for green vegetation cover. The NDVI product contains atmospherically corrected bi-directional surface reflectances masked for water, clouds, and cloud shadows. The EVI uses the blue band to remove residual atmospheric contaminations caused by smoke and sub-pixel thin cirrus clouds, which also introduces uncertainties over tropical areas. The EVI also uses feedback adjustment to minimize canopy background variations and to enhance its sensitivity from sparse to dense vegetation conditions. Global MYD13C1 data are cloud-free spatial composites of the gridded 16-day 1 km MYD13A2, and are provided as a Level 3 product projected on a 0.05° geographic Climate Modeling Grid (CMG). Cloud-free global coverage is achieved by replacing clouds with the historical MODIS time series climatology record.



### 2.2.3 Lidar tree height

This study used global tree height data from Simard et al. (2011). This data set was produced using 2005 data from the Geoscience Laser Altimeter System (GLAS) aboard ICESat (Ice, Cloud, and land Elevation Satellite). The processing follows three steps. First, Simard et al. (2011) developed a procedure to select waveforms and correct slope-induced distortions and to calibrate canopy height estimates using field measurements. In a second step, GLAS canopy height estimations were found to be correlated to other ancillary data such as annual mean precipitation, precipitation seasonality, annual mean temperature, temperature seasonality, elevation, tree cover and classes of protection status. In a second step, a machine learning approach (random forest) was trained using the ancillary variables as input and GLAS tree height as reference data. In the third step, the random forest algorithm was applied to the ancillary data to produce a forest canopy height map at 1 km resolution for areas not covered by GLAS waveforms.

### 2.2.4 Above ground biomass

This study used four static AGB benchmark maps (Baccini et al., 2012; Saatchi et al., 2011; Avitabile et al., 2016; Bouvet et al., 2018) each with specific strengths and limitations to assess L-VOD's ability to reflect aboveground biomass in different biomes: Whereas the maps produced by Saatchi, Baccini and Avitabile aim at covering all pan-tropical region, with focus on dense forests, the Bouvet's map focuses on African savannas with lower biomass values. To take advantage of ALOS/PALSAR L-band observations, in the current study the Bouvet data set has also been extended to rainforest (see below).

The first AGB map over Africa was extracted from the 1 km resolution pan-tropical AGB data set produced by Saatchi et al. (2011). The methodology to produce this data set involves roughly two steps:

(i) in situ inventory plots are used to derive AGB estimates from the Lorey's height (the basal area weighted height of all trees with a diameter of more than 10 cm) calculated from the ICESat GLAS measurements,

(ii) these punctual measurements are spatially extrapolated using MODIS and Quick Scatterometer (QuikSCAT) data through Maximum Entropy (MaxEnt) modeling. All in situ AGB measurements were made from year 1995 to year 2005, and the MODIS and QuikSCAT data used for spatial extrapolation were acquired in 2000-2001, so that the resulting biomass map is representative of AGB circa the year 2000.

This study also used data over Africa extracted from the pan-tropical AGB data set produced by Baccini et al. (2012). The methodology used to produce this data set is very similar to that of Saatchi et al. (2011), except that (i) only MODIS data are used for the spatial extrapolation, (ii) Random Forest is used instead of MaxEnt, (iii) the data set is representative of circa 2007-2008, and (iv) the AGB map is produced at a resolution of 500 m.

The Avitabile et al. (2016) was also used in this study. This forest biomass data set was obtained by merging the data sets by Saatchi et al. (2011) and Baccini et al. (2012) with machine learning techniques to compute a pan-tropical AGB map at 1-km spatial resolution. The merging method was trained using an independent reference data set with field observations and locally calibrated high-resolution biomass maps, harmonized and up-scaled to be representative of 1 km<sup>2</sup>. They used a total of 14477



AGB samples in Australia, Southern Asia, Africa, South America and Central America, spanning AGB values from 0 to ~ 500 Mg/h and covering different biomes such as grasslands, shrublands, savannahs and rainforest.

The fourth biomass map used in this study is based on Bouvet et al. (2018) map over savannas and from Mermoz et al. (2015) over dense forests. The map from Bouvet et al. (2018) at 25 meter resolution is the first biomass map for Africa with focus on savannas and was built from a L-band ALOS PALSAR mosaic produced with observations made in year 2010 (when SMOS was already in operation). A direct model was developed to relate the PALSAR backscatter to AGB with the help of in situ and ancillary data. In a subsequent step, a Bayesian inversion of the direct model was performed. Seasonal effects were taken into account by stratification into wet/dry season areas. In Bouvet et al. (2018), the method was originally applied to savannah and woodlands with typical AGB values of less than 85 Mg/h. In the current study, the Bouvet et al. data set was extended to regions with AGB values larger than 85 Mg/h using the methodology presented by Mermoz et al. (2014): the ESA CCI (Climate Change Initiative) land cover map was used to separate dense forest areas, over which AGB was estimated at 500 meter resolution using the results by Mermoz et al. (2015). The resulting data set will be referred to as the Bouvet-Mermoz data set in the following.

### 3 Methods

The region selected for this study was the African continent because the Bouvet-Mermoz data set, which is the only one that has been produced using SAR observations made in the same frequency band (L-band) as SMOS, is limited to Africa. The African continent contains arid, equatorial and temperate regions (Kottek et al., 2006) with deserts, shrublands, mediterranean woodlands, grasslands, savannah and rainforests (Olson et al., 2001). Therefore, this study covers a wide range of climate regions and biomes and allows to extend the analysis of L-VOD data to monitor vegetation properties, in particular biomass, at larger scales than previous studies (Grant et al., 2016; Lawrence et al., 2014; Vittucci et al., 2015).

AGB, precipitation, tree height, MODIS NDVI/EVI and SMOS L2 data were aggregated and re-sampled to the EASEv2 grid common to the SMOS L3 and IC data sets using the Geospatial Data Abstraction Library (GDAL) routine `gdalwarp` in average mode. Regarding, the SMOS Level 2 data, several SMOS Level 2 retrievals are available for a given day for high northern and southern latitudes. At these latitudes, the best retrievals (corresponding to lower values of the cost function) were selected.

In spite of observing in a protected band dedicated to research observations, some radio frequency interferences (RFI) from human-built equipment affect the quality of the SMOS observations. SMOS L2 and L3 data with low quality (goodness of the fit to the observed brightness temperatures as given by the  $\chi^2$  parameter larger than 3) were filtered out. In the case of SMOS-IC, data with a root mean squared difference between modelled and observed brightness temperatures larger than 10 K were filtered out. In addition, the L-VOD time series of the three products were analysed grid point-to-grid point, and values with a deviation (in absolute value) larger than 2.5 with respect to the grid point average  $\sigma$  (where  $\sigma$  is the standard deviation) were considered as outliers and also filtered out.



The main evaluation strategy used in this study is to spatially compare L-VOD data to the evaluation data sets presented in Sect. 2. These variables such as above ground biomass, tree height, or long-term averages of yearly rainfall are not expected to change quickly over time. Therefore, the L-VOD data were averaged on a yearly basis to avoid short-term variations due to changes in the vegetation water content over short time periods. The biomass data sets discussed in Sect. 2 were produced with observations done from years 1995 to 2010. The comparison of L-VOD with the other data sets was done using L-VOD data computed in 2011, as 2011 is the first complete year after the SMOS commissioning phase, which ended in June 2010.

To get a quantitative assessment of the correlation and the dispersion of L-VOD versus the evaluation data sets, three correlation coefficients were computed. The Pearson correlation coefficient  $R$  is a measure of the linear correlation between two variables. If the relationship linking these variables is linear with no dispersion,  $R$  equals 1 (both variables increase together) or -1 (one variable increases when the other decreases). However, the relationships between L-VOD and the evaluation data are not expected to be linear in most of the cases. Therefore, the Spearman and Kendall rank correlations (which can range from -1 to 1) were also computed to quantify monotonic relationships whether linear or not (more details are provided in the Supp. Information).

The relationships linking L-VOD to the evaluation data for different biomes were fitted using linear fits. In addition, fits to the global relationships linking AGB and L-VOD were computed following the approach used by Liu et al. (2015). The L-VOD data was binned in 0.05-width bins. For each L-VOD bin, the 5th and 95th percentiles and the mean of the AGB distribution were computed, providing three AGB curves as a function of L-VOD. The three curves were fitted with Liu et al. (2015) function, with a logistic function or with a generalized logistic function, obtaining results of the same quality (more details are provided in the Supp. Information).

## 20 4 Results

Figure 1 shows the annual mean for 2011 of the three SMOS L-VOD products and of the MODIS NDVI and EVI indices. It also shows the remaining static data sets after resampling to a 25 km EASEv2 grid, when needed.

### 4.1 Comparison of the three L-VOD data sets

Figure 2 show the scatter plots of SMOS IC L-VOD with respect to the evaluation data. The scatter plots obtained with the L2 and L3 data sets are shown in Figs. S1 and S2, respectively. A visual inspection shows that the scatter plots obtained with IC L-VOD are significantly different than those of L2 and L3 L-VOD, as they show smoother relationships with lower dispersion with respect to all the evaluation data sets than the equivalent plots for L2 and L3 L-VOD.

A quantitative assessment of the correlation and the dispersion of the different scatter plots can be found in Table 1, where Pearson, Spearman and Kendall correlation coefficients are given for the three L-VOD data sets with respect to the evaluation data sets. The lowest correlation coefficient values were obtained for L3 L-VOD ( $R = 0.65 - 0.87$ ). The correlation coefficients obtained for L2 L-VOD are similar ( $R = 0.67 - 0.87$ ) than those obtained for L3 L-VOD but systematically higher by up to 4%. The values obtained for IC L-VOD are the highest ( $R = 0.77 - 0.94$ ) with respect to all the evaluation data sets. The correlation



increases is in the range of 5%-10% with respect to L2 L-VOD and up to 15 % with respect to L3 L-VOD. Therefore, using eight vegetation-related evaluation data sets, the most consistent SMOS L-VOD data set is SMOS-IC.

#### 4.2 Comparison of SMOS IC L-VOD to other data sets

Taking into account that the best results presented in Sect. 4.1 were obtained with SMOS-IC L-VOD, only the latter is considered in the following. The relationship between tree height and IC L-VOD was found to be close to linear with a high Pearson correlation coefficient ( $R = 0.87$ , Table 1), in agreement with previous findings using SMOS L2 data Rahmoune et al. (2013).

With respect to visible/infra-red indices such as EVI and NDVI, Figure 2 shows that both indices saturate even for moderate L-VOD values of  $\sim 0.5$ , in agreement with previous studies (Lawrence et al., 2014). The correlation coefficients are  $R = 0.80 - 0.81$  and  $\rho = 0.86 - 0.88$  for NDVI and EVI. Regarding precipitation, the scatter plots show more dispersion ( $R = 0.77$ ,  $\rho = 0.82$ ) than those obtained with NDVI and EVI but there is a saturation in the mean annual cumulated precipitation values for L-VOD values higher than  $\sim 0.6 - 0.7$ .

Regarding the different AGB data sets, most of the scatter plots show a clear non-linear relationship between L-VOD and AGB. However, the relationship between Baccini et al. (2012) AGB versus IC L-VOD is almost linear for the whole range of L-VOD and AGB values and the associated Pearson correlation coefficients are the highest found ( $R = 0.94$ ,  $\rho = 0.90$ ). The relationship between Avitabile et al. (2016) AGB and L-VOD is the most non-linear one ( $R = 0.85$ ,  $\rho = 0.84$ ). It shows a low sensitivity to low L-VOD values and a large dispersion for high L-VOD values with AGB ranging from  $\sim 300$  Mg/h to 500 Mg/h. The relationship between L-VOD and the Bouvet-Mermoz AGB data set ( $R = 0.89$ ,  $\rho = 0.91$ ) also shows a large dispersion for high L-VOD values with AGB spanning a range from 200 to 400 Mg/h. In contrast, the results obtained with the Saatchi et al. (2011) ( $R = 0.92$ ,  $\rho = 0.91$ ) and Baccini et al. (2012) data sets show a single AGB peak for the highest SMOS L-VOD values with values of  $\sim 280$  Mg/h and  $\sim 320$  Mg/h, respectively. Interestingly, the Bouvet-Mermoz AGB data set, which has been obtained from L-band SAR data and is the only one developed with a particular focus on savannahs, shows a linear relationship between L-VOD and AGB with a very low dispersion for low L-VOD and AGB values. In summary, IC L-VOD shows a high sensitivity to AGB, with smooth relationships without strong signs of saturation, in particular with respect to the AGB data sets from Saatchi et al. (2011), Baccini et al. (2012) and Bouvet-Mermoz.

#### 4.3 Comparison of IC L-VOD to other data sets per land cover class

To get further insight into the relationship of SMOS IC L-VOD and the evaluation data sets, an analysis per IGBP land cover class was performed. Figure 3 shows the relationships in between L-VOD and Bouvet-Mermoz AGB, tree height, NDVI and precipitations for two groups of biomes using the IGBP land cover classification: (i) evergreen broadleaf, and (ii) all other biomes (grasslands, croplands, shrublands, savannahs and woody savannahs). Figure S5 shows the spatial distribution of those two groups in the Bouvet-Mermoz map. Each panel of Fig. 3 shows the regression line, and the Pearson  $R$ , Spearman  $\rho$  and Kendall  $\tau$  coefficients. Figure S6 shows scatter plots of SMOS-IC L-VOD with respect to the four AGB data sets and the tree height data computed for more specific land cover classes.



Maximum L-VOD values increase from grasslands, croplands and shrublands to savannahs and woody savannahs, where L-VOD reaches a maximum value of  $\sim 0.7$ . The slope of the NDVI and L-VOD relationships for these biomes decreases smoothly and therefore the global relationship is non-linear. The slope is close to zero for evergreen broadleaf rainforest.

Although with a significant dispersion, the scatter plot of L-VOD and the cumulated precipitations outside the rainforest shows a close to linear relationship, with the cumulated precipitations increasing up to  $\sim 1700$  mm for L-VOD  $\sim 0.7$ . As the relationship with NDVI, the slope of the precipitations and L-VOD relationship for the rainforest is low.

The scatter plot of tree height and L-VOD shows a similar slope out and within the rainforest, giving the global linear relationship showed in Fig. 2. Out of the rainforest, the maximum tree height value is  $\sim 20$  m for L-VOD  $\sim 0.7$ .

The scatter plots showing the Bouvet-Mermoz AGB and L-VOD relationship shows a linear relationship out and within the rainforest. It is noteworthy that out of the rainforest, the relationship of L-VOD and AGB is the one showing the lowest dispersion ( $\rho = 0.87$ ,  $\tau = 0.68$ ) of all the evaluation data sets. Therefore, for African shrublands, grasslands, croplands and savannahs, the SMOS L-VOD data is in very good agreement with the independent AGB map obtained from L-band SAR observations by Bouvet et al. (2018). The 0-85 Mg/h range estimated by Bouvet et al. in these regions corresponds to the 0-0.7 L-VOD range, where the vegetation characteristics seem to be closely related to the amount of annual precipitations. In contrast to tree height, the slope of the AGB and L-VOD relationship increases by a factor of  $\sim 2$  in the rainforest, giving the global non-linear relationship shown in Fig. 2. The comparison of L-VOD to other AGB datasets for different biomes shows a behaviour consistent to that found with the Bouvet-Mermoz data set (Supp. Information).

#### 4.4 Sensitivity of L-VOD to AGB and comparison to other indices

To get further insight into the global AGB versus L-VOD relationship, the fitting method described in Sect. 3 was used. Figure S3 shows the fits using a logistic function and Table S2 shows the best-fit parameters.

Since Liu et al. (2015) discussed fits of Saatchi's AGB as a function K/X/C-VOD, in order to compare the performance of NDVI, K/X/C-VOD and L-VOD to estimate AGB, the Saatchi data set was used. The scatter plot between Saatchi's AGB and NDVI was fitted using the method described in Sect. 3 and the fits to the 5th and 95th percentiles curves were plotted in Fig. 4. In addition, Fig. 4 shows the fits obtained by Liu et al. (2015) to the 5th and 95th percentiles curves of Saatchi's AGB versus K/X/C-VOD. Finally, Fig. 4 also shows the fits to Saatchi's AGB 5th and 95th percentiles curves as a function of SMOS-IC L-VOD. For each data set, the area inside the 5th and 95th percentile fits was shaded. For ease of comparison, VOD and NDVI were normalized from 0 to 1 using their respective maximum values.

As expected, NDVI shows some sensitivity to AGB only for low AGB values (with a low slope) before showing a strong saturation for AGB values higher than  $\sim 70$  Mg/h. The relationship between AGB and K/X/C-VOD shows a similar shape to that of AGB versus NDVI but it is slightly shifted to lower normalized VOD values. AGB increases from  $\sim 50$  Mg/h to  $\sim 300$  Mg/h for K/X/C-VOD values higher than 70 % of their total value. In contrast, the relationship between AGB and L-VOD shows a more steady increase from low to high AGB and L-VOD values. In particular, it does not show a threshold beyond which the relationship saturates and the slope increases significantly.



## 5 Discussion

As mentioned in Sect. 2, SMOS L2 and L3 products consider heterogeneous land covers inside the SMOS footprints, while SMOS-IC does not account for footprint heterogeneity. The better results obtained with the SMOS-IC data set suggests that the approach used to account for heterogeneous land covers introduce uncertainties in the Level 2 and 3 products. Nevertheless, independently of the choice of the SMOS L-VOD data set, the results showed a generally high sensitivity of L-VOD with respect to the vegetation-related variables/indices used for the evaluation, in particular with respect to AGB ( $R = 0.78 - 0.94$ ).

The relationship between tree height and SMOS L-VOD was found to be close to linear, confirming previous findings by Rahmoune et al. (2014) using SMOS L2 L-VOD. Vittucci et al. (2015) estimated a correlation of L2 L-VOD and tree height of 0.81, which is in good agreement with the value reported here ( $R = 0.79$ , Table 1). However, for IC L-VOD the relationship was found to be closer to a linear one, with less dispersion and a significantly higher correlation ( $R = 0.87$ ).

The SMOS-IC L-VOD relationships with respect to NDVI and EVI were found in agreement with those discussed using SMOS L3 data by Grant et al. (2016) as there is a saturation in EVI and NDVI for high L-VOD values. In contrast, the relationships found in this study using SMOS-IC showed less dispersion than those found by Grant et al. (2016).

Regarding the comparison to AGB, Vittucci et al. (2015) discussed the relationship linking L2 L-VOD and biomass from the Carnegie Airborne Observatory (Asner et al., 2014) at 20 selected points over Peru, Columbia, and Panama spanning AGBs from  $\sim 50$  Mg/h to  $\sim 280$  Mg/h. The relationship was almost linear, in good agreement with the results discussed in Sect. 4 for SMOS IC L-VOD for evergreen broadleaf forest.

## 6 Conclusions

Three different SMOS-based L-VOD data sets were evaluated and compared to precipitation, tree height, NDVI, EVI and AGB data. Lower dispersion and smoother relationships were obtained by using SMOS-IC L-VOD, compared to the L2 and L3 L-VOD data sets. Consistently, the rank correlation values obtained with SMOS-IC were significantly higher by 5-15 % than those obtained with Level 2 and Level 3 L-VOD data sets.

The relationships between AGB estimates and L-VOD were strong ( $R = 0.85 - 0.94$ ) but differed among the products. For low vegetation classes (grasslands to woody savannah), the best performance was achieved with the Bouvet's savannah biomass data set. The biomass data produced by Baccini and Saatchi performed well for all vegetation classes and show the best agreement with L-VOD for dense forest ( $R = 0.70 - 0.79$ ). Avitabile's AGB data showed low correlation values with L-VOD for low vegetation classes and a similar performance to Bouvet-Mermoz for dense forest ( $R = 0.64 - 0.67$ ). Furthermore, we found a linear relationship for the Baccini data which was not the case for the remaining data. The AGB and L-VOD relationships can be fitted over the entire range of both variables with a single law using a sigmoid logistic function. However, an analysis per land cover class showed that within the same class, the L-VOD and AGB relationship is linear also for the Saatchi et al. (2011); Avitabile et al. (2016) and Bouvet-Mermoz data sets. Therefore, the global non-linear relationship, found when all the different land cover are considered together, arises from different slopes in the L-VOD/AGB relationship obtained



for different land cover classes considered separately. For low vegetation classes, the annual mean of L-VOD spans a range from 0 to 0.7 and it shows a linear relationship with the amount of the average annual precipitations.

The relationship between AGB versus L-VOD was compared to the ones between AGB versus NDVI and AGB versus K/X/C-VOD from Liu et al. (2015). As expected, NDVI saturates strongly and it becomes weakly sensitive to AGB changes from  $\sim 70$  to  $\sim 300$  Mg/h. With respect to K/X/C-VOD, the AGB also increases slowly as VOD increases for most ( $\sim 70$  %) of the K/X/C-VOD dynamic range but it saturates more gradually than for NDVI. In contrast, AGB values show a steady increment as L-VOD increases over the whole L-VOD dynamic range.

The equations computed in this study can be used to estimate AGB from SMOS-IC L-VOD. Of course, these equations depend on the data set used as reference to fit the AGB and L-VOD relationship. Three of them (those determined with Baccini et al. (2012), Saatchi et al. (2011) and Bouvet-Mermoz) gave very similar values when the 5th and 95th percentiles of the distributions were taken into account.

The results obtained in this study showed that the L-VOD parameter estimated from the SMOS passive microwave observations is an interesting index to monitor AGB at coarse resolution ( $\sim 40$  km). The advantage of this technique is that it allows to add a temporal dimension to the static AGB maps estimated from other remote sensing observations with high spatial resolution. Despite its coarse spatial resolution, the high temporal resolution of the new SMOS L-VOD data will be useful to perform temporal estimations of the changes in the global carbon stocks at large scales.

*Author contributions.* NJRF, AM, YK and JPW planned the research discussed in this manuscript and NJRF and AM performed most the computations. SM, AB and TLT provided the AGB data sets and expertise on AGB estimations. AM, JPW and AAY provided the SMOS-IC data. PR preprocessed the SMOS Level 2 data. TK, AAB and MB reviewed the system design and the results, in particular regarding the analysis per land cover classes. All authors participated in the writing and provided comments and suggestions.

*Competing interests.* The authors declare that they have no conflict of interest.

*Acknowledgements.* N.J.R.-F, J.-P.W, T.K., A.M. and Y.H.K. acknowledge partial support by the ESA contract No. 4000117645/16/NL/SW Support To Science Element SMOS+Vegetation and by CNES (Centre National d'Etudes Spatiales) TOSCA program. They also acknowledge and interesting discussions with other colleagues involved in the SMOS+Vegetation project (Marko Scholze, Matthias Drusch, Michael Vossbeck, Wolfgang Knorr, Cristina Vitucci and Paolo Ferrazzoli). SMOS Level 3 data were obtained from the "Centre Aval de Traitement des Données SMOS" (CATDS), operated for the CNES (France) by IFREMER (Brest, France).

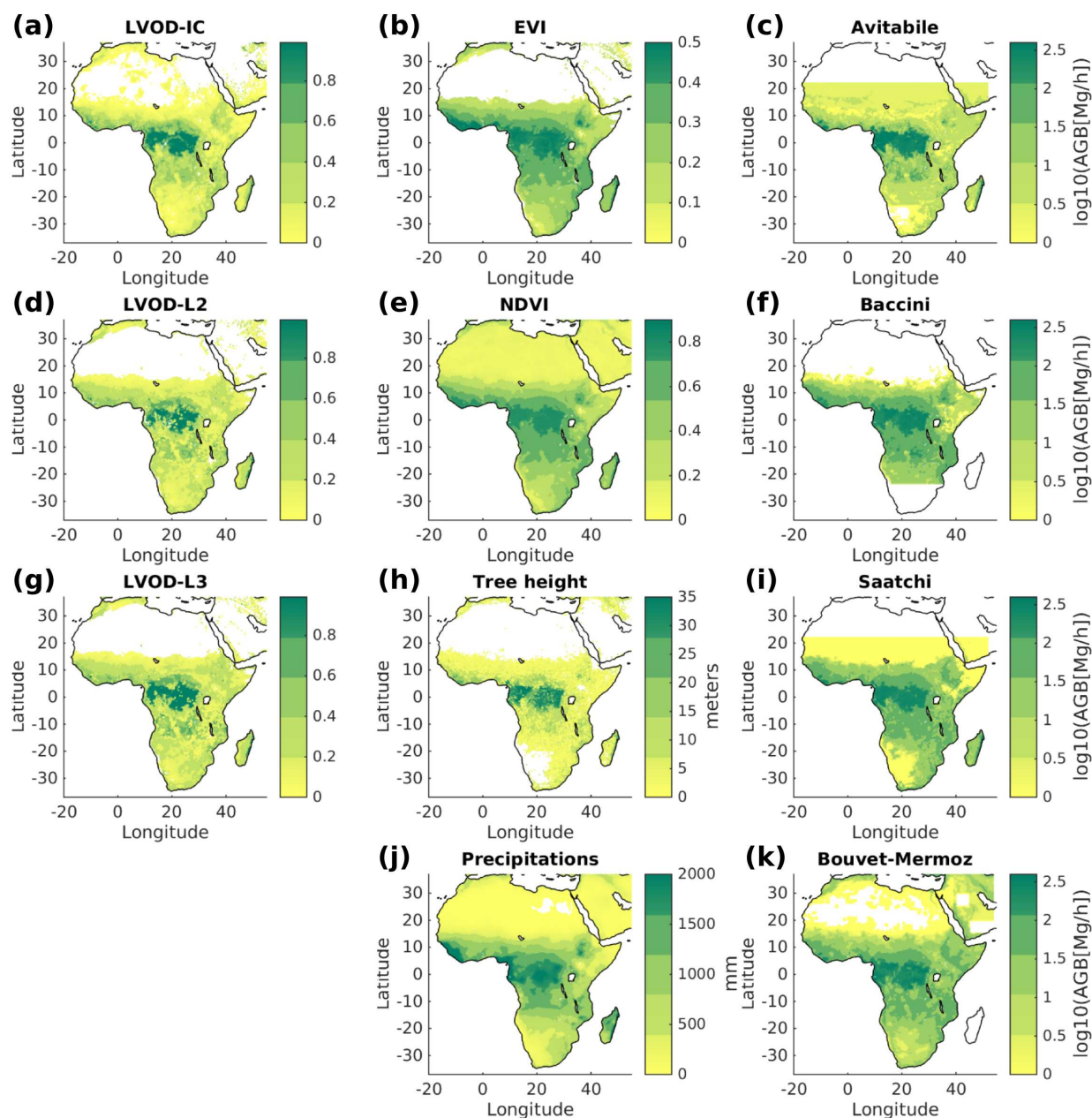


**Figure 1.** Year 2011 annual mean of L-VOD for the SMOS-IC, SMOS L2 and SMOS L3 (panels **a**, **d** and **g**, respectively). Data used to evaluate the SMOS L-VOD datasets (middle and right panels). Year (2011) average of MODIS EVI (**b**) and NDVI (**e**). Simard et al. (2011) tree height (**h**). Worldclim average annual precipitations (**j**). AGB maps from Avitabile et al. (2016), Baccini et al. (2012), Saatchi et al. (2011) and Bouvet et al. (2018) (panels **c**, **f**, **i**, **k**, respectively)

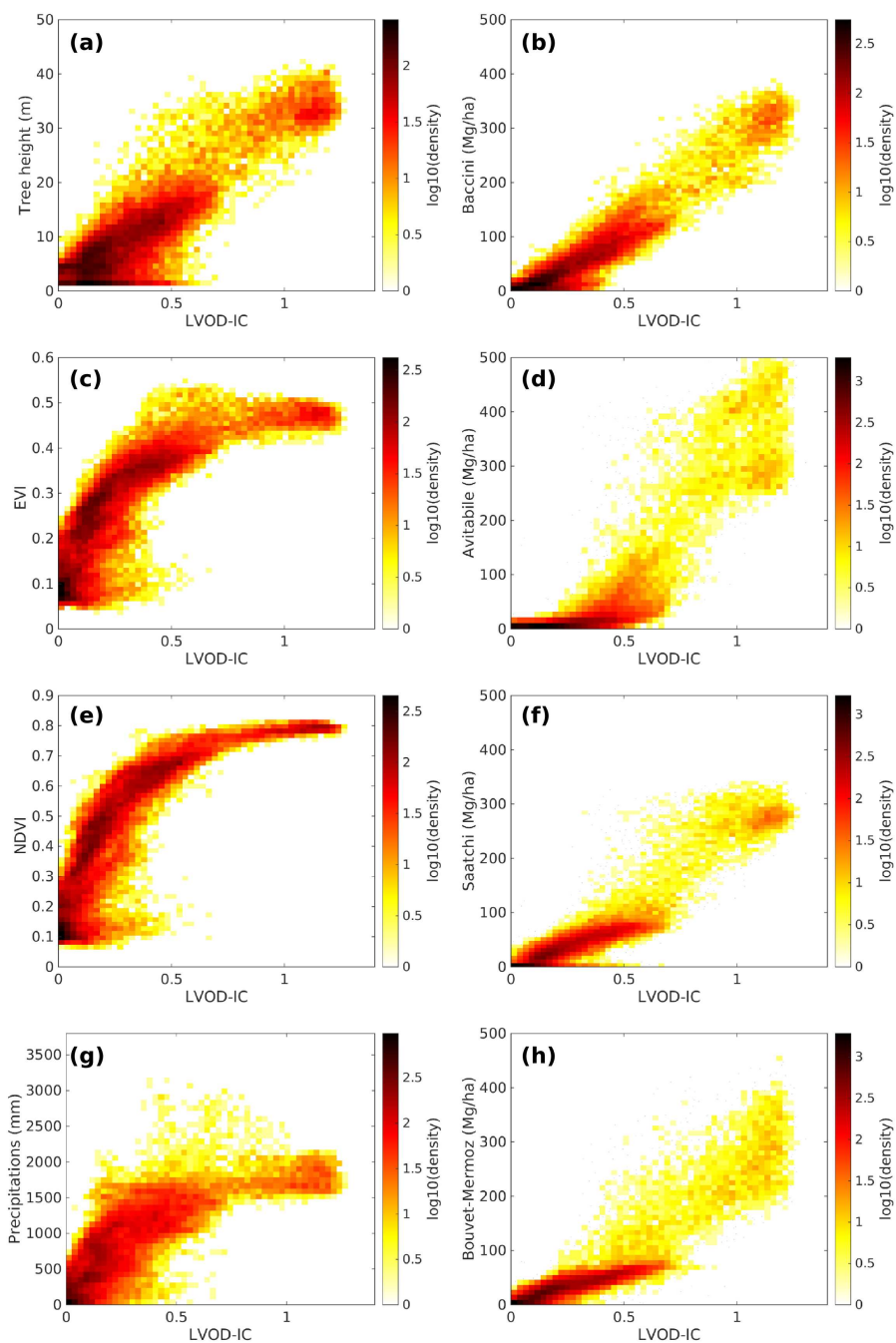


**Figure 2.** Density scatter plots of SMOS-IC L-VOD respect to: tree height (a), EVI (c), NDVI (e), cumulated precipitation (g), Baccini et al. (2012) AGB (b), Avitabile et al. (2016) AGB (d), Saatchi et al. (2011) AGB (f) and Bouvet-Mermoz AGB datasets (h).



**Table 1.** Pearson's  $R$ , Spearman's  $\rho$  and Kendal's  $\tau$  correlation coefficients of the three SMOS L-VOD data sets with respect to cumulated precipitations, tree height, MODIS NDVI and EVI and AGB from Saatchi et al. (2011), Avitabile et al. (2016), Baccini et al. (2012) and Bouvet-Mermoz.

	$R$			$\rho$			$\tau$		
	IC	L2	L3	IC	L2	L3	IC	L2	L3
Precipitations	0.77	0.67	0.65	0.82	0.72	0.69	0.62	0.53	0.50
Tree Height	0.87	0.79	0.78	0.78	0.67	0.66	0.61	0.50	0.49
NDVI	0.81	0.75	0.73	0.88	0.81	0.78	0.72	0.63	0.60
EVI	0.80	0.74	0.73	0.86	0.79	0.76	0.69	0.60	0.57
Avitabile	0.85	0.78	0.78	0.84	0.73	0.72	0.65	0.54	0.53
Baccini	0.94	0.87	0.87	0.90	0.80	0.77	0.74	0.62	0.60
Saatchi	0.92	0.84	0.84	0.91	0.82	0.80	0.75	0.64	0.62
Bouvet-Mermoz	0.89	0.81	0.81	0.91	0.83	0.80	0.75	0.65	0.62

## References

- Al Bitar, A., Mialon, A., Kerr, Y., Cabot, F., Richaume, P., Jacquette, E., Quesney, A., Mahmoodi, A., Tarot, S., Parrens, M., Al-yaari, A., Pel-  
 5 larin, T., Rodriguez-Fernandez, N., and Wigneron, J.-P.: The Global SMOS Level 3 daily soil moisture and brightness temperature maps, *Earth System Science Data*, 9, 293–315, <https://doi.org/10.5194/essd-2017-1>, <http://www.earth-syst-sci-data-discuss.net/essd-2017-1/>, 2017.
- Andela, N., Liu, Y., Van Dijk, A., De Jeu, R., and McVicar, T.: Global changes in dryland vegetation dynamics (1988-2008) assessed by  
 satellite remote sensing: Comparing a new passive microwave vegetation density record with reflective greenness data, *Biogeosciences*,  
 10, 6657, 2013.
- Asner, G. P., Knapp, D. E., Martin, R. E., Tupayachi, R., Anderson, C. B., Mascaro, J., Sinca, F., Chadwick, K. D., Higgins, M., Farfan,  
 10 W., Llactayo, W., and Silman, M. R.: Targeted carbon conservation at national scales with high-resolution monitoring, *Proceedings of the  
 National Academy of Sciences*, 111, E5016–E5022, <https://doi.org/10.1073/pnas.1419550111>, 2014.
- Avitabile, V., Herold, M., Heuvelink, G., Lewis, S. L., Phillips, O. L., Asner, G. P., Armston, J., Ashton, P. S., Banin, L., Bayol, N., et al.: An  
 integrated pan-tropical biomass map using multiple reference datasets, *Global change biology*, 2016.
- Baccini, A., Goetz, S., Walker, W., Laporte, N., Sun, M., Sulla-Menashe, D., Hackler, J., Beck, P., Dubayah, R., Friedl, M., et al.: Estimated  
 15 carbon dioxide emissions from tropical deforestation improved by carbon-density maps, *Nature Climate Change*, 2, 182–185, 2012.
- Bouvet, A., Mermoz, S., Toan, T. L., Villard, L., Mathieu, R., Naidoo, L., and Asner, G. P.: An above-ground biomass map of African  
 savannahs and woodlands at 25 m resolution derived from {ALOS} {PALSAR}, *Remote Sensing of Environment*, 206, 156 – 173,  
<https://doi.org/https://doi.org/10.1016/j.rse.2017.12.030>, <https://www.sciencedirect.com/science/article/pii/S0034425717306053>, 2018.
- Brandt, M., Rasmussen, K., Peñuelas, J., Tian, F., Schurgers, G., Verger, A., Mertz, O., Palmer, J. R., and Fensholt, R.: Human population  
 20 growth offsets climate-driven increase in woody vegetation in sub-Saharan Africa, *Nature Ecology & Evolution*, 1, 0081, 2017.

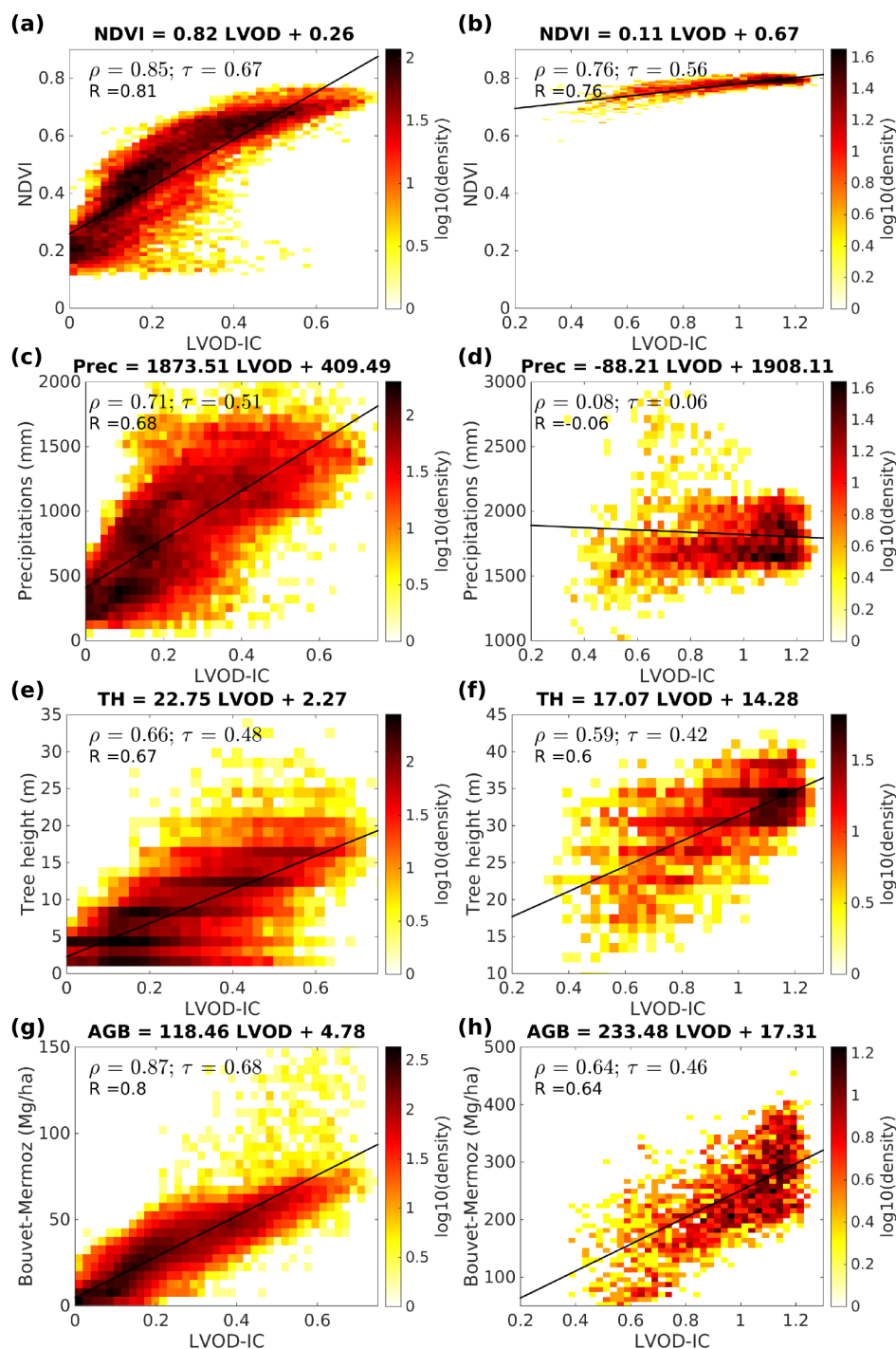


**Figure 3.** SMOS IC L-VOD relationships to NDVI (a, b), precipitations (c, d), tree height (e, f) and Bouvet-Mermoz AGB (g, h) for two biome groups. Panels a, c, e, g represent the results including shrublands, croplands, natural vegetation and grasslands, savannah and woody savannah. Panels b, d, f, h show the results for evergreen broadleaf rainforest.

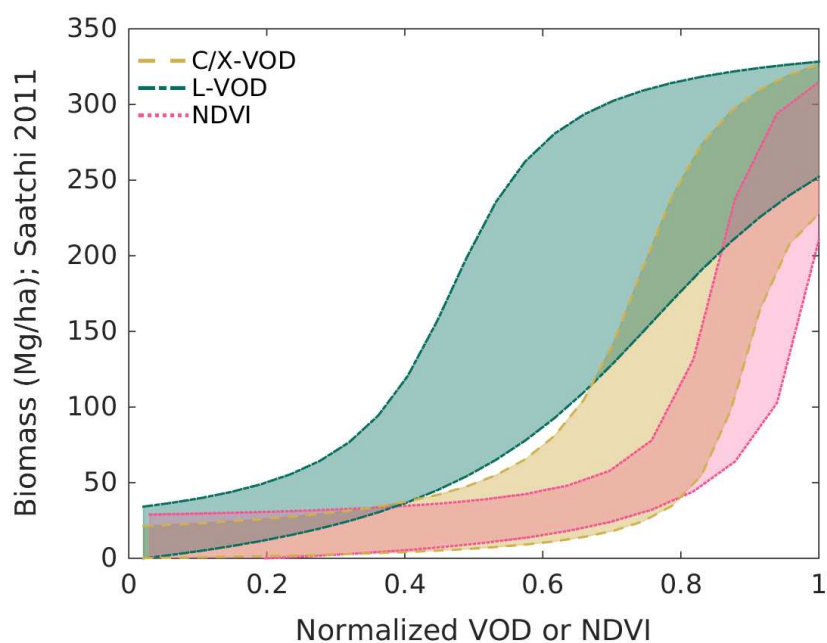


**Figure 4.** Fits of the 5th and 95th percentile curves of the Saatchi et al. (2011) AGB with respect to SMOS-IC L-VOD (green), K/X/C-VOD from Liu et al. (2015) (brown), and NDVI (pink). The VOD and NDVI distributions were normalized from 0 to 1 using their respective maxima.

Brodzik, M. J., Billingsley, B., Haran, T., Raup, B., and Savoie, M. H.: EASE-Grid 2.0: Incremental but Significant Improvements for Earth-Gridded Data Sets., *ISPRS International Journal of Geo-Information*, 1(1), 32–45, <https://doi.org/doi:10.3390/ijgi1010032>, <http://www.mdpi.com/2220-9964/1/1/32/>, 2012.

Entekhabi, D., Njoku, E. G., O'Neill, P. E., Kellogg, K. H., Crow, W. T., Edelstein, W. N., Entin, J. K., Goodman, S. D., Jackson, T. J., Johnson, J., et al.: The soil moisture active passive (SMAP) mission, *Proceedings of the IEEE*, 98, 704–716, 2010.

Esau, I., Miles, V. V., Davy, R., Miles, M. W., and Kurchatova, A.: Trends in normalized difference vegetation index (NDVI) associated with urban development in northern West Siberia, *Atmospheric Chemistry and Physics*, 16, 9563–9577, 2016.

Fernandez-Moran, R., Al-Yaari, A., Mialon, A., Mahmoodi, A., Al Bitar, A., De Lannoy, G., Rodriguez-Fernandez, N., Lopez-Baeza, E., Kerr, Y., and Wigneron, J.-P.: SMOS-IC: An alternative SMOS soil moisture and vegetation optical depth product, *Remote Sensing*, 9, 457, 2017.

Ferrazzoli, P. and Guerriero, L.: Passive microwave remote sensing of forests: A model investigation, *IEEE Transactions on Geoscience and Remote Sensing*, 34, 433–443, 1996.

Grant, J., Wigneron, J.-P., De Jeu, R., Lawrence, H., Mialon, A., Richaume, P., Al Bitar, A., Drusch, M., van Marle, M., and Kerr, Y.: Comparison of SMOS and AMSR-E vegetation optical depth to four MODIS-based vegetation indices, *Remote Sensing of Environment*, 172, 87–100, 2016.



- Herrmann, S. M., Anyamba, A., and Tucker, C. J.: Recent trends in vegetation dynamics in the African Sahel and their relationship to climate, *Global Environmental Change*, 15, 394–404, 2005.
- Hornbuckle, B. K., England, A. W., De Roo, R. D., Fischman, M. A., and Boprie, D. L.: Vegetation canopy anisotropy at 1.4 GHz, *IEEE Transactions on Geoscience and Remote Sensing*, 41, 2211–2223, 2003.
- 5 Huete, A., Didan, K., Miura, T., Rodriguez, E. P., Gao, X., and Ferreira, L. G.: Overview of the radiometric and biophysical performance of the MODIS vegetation indices, *Remote sensing of environment*, 83, 195–213, 2002.
- Jackson, T. and Schmugge, T.: Vegetation effects on the microwave emission of soils, *Remote Sensing of Environment*, 36, 203–212, 1991.
- Jung, M., Reichstein, M., Margolis, H. A., Cescatti, A., Richardson, A. D., Arain, M. A., Arneeth, A., Bernhofer, C., Bonal, D., Chen, J., et al.: Global patterns of land-atmosphere fluxes of carbon dioxide, latent heat, and sensible heat derived from eddy covariance, satellite,  
10 and meteorological observations, *Journal of Geophysical Research: Biogeosciences*, 116, 2011.
- Kerr, Y., Waldteufel, P., Wigneron, J.-P., Delwart, S., Cabot, F., Boutin, J., Escorihuela, M.-J., Font, J., Reul, N., Gruhier, C., Juglea, S., Drinkwater, M., Hahne, A., Martin-Neira, M., and Mecklenburg, S.: The SMOS Mission: New Tool for Monitoring Key Elements of the Global Water Cycle, *Proceedings of the IEEE*, 98, 666–687, <https://doi.org/10.1109/JPROC.2010.2043032>, 2010.
- Kerr, Y., Waldteufel, P., Richaume, P., Wigneron, J., Ferrazzoli, P., Mahmoodi, A., Al Bitar, A., Cabot, F., Gruhier, C., Juglea, S., Leroux, D.,  
15 Mialon, A., and Delwart, S.: The SMOS Soil Moisture Retrieval Algorithm, *IEEE Transactions on Geoscience and Remote Sensing*, 50, 1384–1403, <https://doi.org/10.1109/TGRS.2012.2184548>, 2012.
- Kerr, Y. H., Waldteufel, P., Wigneron, J. P., Martinuzzi, J., Font, J., and Berger, M.: Soil moisture retrieval from space: the Soil Moisture and Ocean Salinity (SMOS) mission, *IEEE Transactions on Geoscience and Remote Sensing*, 39, 1729–1735, <https://doi.org/10.1109/36.942551>, 2001.
- 20 Kirdiashev, K., Chukhlantsev, A., and Shutko, A.: Microwave radiation of the earth's surface in the presence of vegetation cover, *Radiotekhnika I Elektronika*, 24, 256–264, 1979.
- Kottek, M., Grieser, J., Beck, C., Rudolf, B., and Rubel, F.: World map of the Köppen-Geiger climate classification updated, *Meteorologische Zeitschrift*, 15, 259–263, 2006.
- Lawrence, H., Wigneron, J.-P., Richaume, P., Novello, N., Grant, J., Mialon, A., Bitar, A. A., Merlin, O., Guyon, D., Leroux, D., Bircher, S., and Kerr, Y.: Comparison between {SMOS} Vegetation Optical Depth products and {MODIS} vegetation indices over crop zones of the {USA}, *Remote Sensing of Environment*, 140, 396 – 406, <https://doi.org/http://dx.doi.org/10.1016/j.rse.2013.07.021>, <http://www.sciencedirect.com/science/article/pii/S0034425713002332>, 2014.
- Liu, Y., de Jeu, R. A., van Dijk, A. I., and Owe, M.: TRMM-TMI satellite observed soil moisture and vegetation density (1998–2005) show strong connection with El Niño in eastern Australia, *Geophysical Research Letters*, 34, 2007.
- 30 Liu, Y. Y., de Jeu, R. A., McCabe, M. F., Evans, J. P., and van Dijk, A. I.: Global long-term passive microwave satellite-based retrievals of vegetation optical depth, *Geophysical Research Letters*, 38, 2011.
- Liu, Y. Y., van Dijk, A. I. J. M., de Jeu, R. a. M., Canadell, J. G., McCabe, M. F., Evans, J. P., and Wang, G.: Recent reversal in loss of global terrestrial biomass: supplementary information, *Nature Climate Change*, 5, 1–5, <https://doi.org/10.1038/nclimate2581>, <http://www.nature.com/doi/10.1038/nclimate2581>, 2015.
- 35 Mermoz, S., Le Toan, T., Villard, L., Réjou-Méchain, M., and Seifert-Granzin, J.: Biomass assessment in the Cameroon savanna using ALOS PALSAR data, *Remote sensing of environment*, 155, 109–119, 2014.
- Mermoz, S., Réjou-Méchain, M., Villard, L., Le Toan, T., Rossi, V., and Gourlet-Fleury, S.: Decrease of L-band SAR backscatter with biomass of dense forests, *Remote Sensing of Environment*, 159, 307–317, 2015.



- Mo, T., Choudhury, B., Schmugge, T., Wang, J., and Jackson, T.: A model for microwave emission from vegetation-covered fields, *Journal of Geophysical Research: Oceans*, 87, 11 229–11 237, 1982.
- Olson, D. M., Dinerstein, E., Wikramanayake, E. D., Burgess, N. D., Powell, G. V., Underwood, E. C., D’amico, J. A., Itoua, I., Strand, H. E., Morrison, J. C., et al.: Terrestrial Ecoregions of the World: A New Map of Life on Earth: A new global map of terrestrial ecoregions provides an innovative tool for conserving biodiversity, *BioScience*, 51, 933–938, 2001.
- 5 Pettorelli, N., Vik, J. O., Mysterud, A., Gaillard, J.-M., Tucker, C. J., and Stenseth, N. C.: Using the satellite-derived NDVI to assess ecological responses to environmental change, *Trends in ecology & evolution*, 20, 503–510, 2005.
- Pettorelli, N., Ryan, S., Mueller, T., Bunnefeld, N., Jędrzejewska, B., Lima, M., and Kausrud, K.: The Normalized Difference Vegetation Index (NDVI): unforeseen successes in animal ecology, *Climate Research*, 46, 15–27, 2011.
- 10 Rahmoune, R., Ferrazzoli, P., Kerr, Y. H., and Richaume, P.: SMOS level 2 retrieval algorithm over forests: Description and generation of global maps, *IEEE Journal of Selected Topics in Applied Earth Observations and Remote Sensing*, 6, 1430–1439, <https://doi.org/10.1109/JSTARS.2013.2256339>, 2013.
- Rahmoune, R., Ferrazzoli, P., Singh, Y., Kerr, Y., Richaume, P., and Al Bitar, A.: SMOS Retrieval Results Over Forests: Comparisons With Independent Measurements, *Selected Topics in Applied Earth Observations and Remote Sensing, IEEE Journal of*, 6-3, 1430 – 1439, <https://doi.org/10.1109/JSTARS.2014.2321027>, 2014.
- 15 Saatchi, S. S., Harris, N. L., Brown, S., Lefsky, M., Mitchard, E. T., Salas, W., Zutta, B. R., Buermann, W., Lewis, S. L., Hagen, S., et al.: Benchmark map of forest carbon stocks in tropical regions across three continents, *Proceedings of the National Academy of Sciences*, 108, 9899–9904, 2011.
- Sahr, K., White, D., and Kimerling, A. J.: Geodesic discrete global grid systems cartography., *Cartography and Geographic Information Science*, 30(2), 30(2), 121–134, 2003.
- 20 Schwank, M., Matzler, C., Guglielmetti, M., and Fluhler, H.: L-band radiometer measurements of soil water under growing clover grass, *IEEE Transactions on Geoscience and Remote Sensing*, 43, 2225–2237, 2005.
- Simard, M., Pinto, N., Fisher, J. B., and Baccini, A.: Mapping forest canopy height globally with spaceborne lidar, *Journal of Geophysical Research: Biogeosciences*, 116, 2011.
- 25 Todd, S., Hoffer, R., and Milchunas, D.: Biomass estimation on grazed and ungrazed rangelands using spectral indices, *International journal of remote sensing*, 19, 427–438, 1998.
- Tucker, C. J.: Red and photographic infrared linear combinations for monitoring vegetation, *Remote sensing of Environment*, 8, 127–150, 1979.
- Ulaby, F.: *Passive microwave remote sensing of the Earth’s surface*, Antennas and Propagation, 1976.
- 30 Ulaby, F. T. and Wilson, E. A.: Microwave attenuation properties of vegetation canopies, *IEEE Transactions on Geoscience and Remote Sensing*, pp. 746–753, 1985.
- Van de Griend, A. A. and Wigneron, J.-P.: The b-factor as a function of frequency and canopy type at H-polarization, *IEEE Transactions on Geoscience and Remote Sensing*, 42, 786–794, 2004.
- Van der Werf, G. R., Randerson, J. T., Giglio, L., Collatz, G., Mu, M., Kasibhatla, P. S., Morton, D. C., DeFries, R., Jin, Y. v., and van Leeuwen, T. T.: Global fire emissions and the contribution of deforestation, savanna, forest, agricultural, and peat fires (1997–2009), *Atmospheric Chemistry and Physics*, 10, 11 707–11 735, 2010.
- 35 Van Marle, M., Van Der Werf, G., de Jeu, R., and Liu, Y.: Annual South American forest loss estimates based on passive microwave remote sensing (1990–2010), *Biogeosciences*, 13, 609, 2016.



- Vicente-Serrano, S. M., Gouveia, C., Camarero, J. J., Beguería, S., Trigo, R., López-Moreno, J. I., Azorín-Molina, C., Pasho, E., Lorenzo-Lacruz, J., Revuelto, J., et al.: Response of vegetation to drought time-scales across global land biomes, *Proceedings of the National Academy of Sciences*, 110, 52–57, 2013.
- Vittucci, C., Ferrazzoli, P., Kerr, Y., Richaume, P., Guerriero, L., Rahmoune, R., and Laurin, G. V.: SMOS retrieval over  
5 forests: Exploitation of optical depth and tests of soil moisture estimates, *Remote Sensing of Environment*, 180, 115–127, <https://doi.org/10.1016/j.rse.2016.03.004>, <http://dx.doi.org/10.1016/j.rse.2016.03.004>, 2015.
- Wigneron, J.-P., Chanzy, A., Calvet, J.-C., and Bruguier, N.: A simple algorithm to retrieve soil moisture and vegetation biomass using passive microwave measurements over crop fields, *Remote Sensing of Environment*, 51, 331–341, 1995.
- Wigneron, J.-P., Pardé, M., Waldteufel, P., Chanzy, A., Kerr, Y., Schmidl, S., and Skou, N.: Characterizing the dependence of vegetation  
10 model parameters on crop structure, incidence angle, and polarization at L-band, *Geoscience and Remote Sensing, IEEE Transactions on*, 42, 416–425, 2004.
- Wigneron, J.-P., Kerr, Y., Waldteufel, P., Saleh, K., Escorihuela, M.-J., Richaume, P., Ferrazzoli, P., de Rosnay, P., Gurney, R., Calvet, J.-C., Grant, J., Guglielmetti, M., Hornbuckle, B., Mätzler, C., Pellarin, T., and Schwank, M.: L-band Microwave Emission of the Biosphere (L-MEB) Model: Description and calibration against experimental data sets over crop fields, *Remote Sensing of Environment*, 107, 639 – 655,  
15 <https://doi.org/https://doi.org/10.1016/j.rse.2006.10.014>, <http://www.sciencedirect.com/science/article/pii/S0034425706004238>, 2007.